PERGAMON

International Journal of Multiphase Flow 28 (2002) 1837–1851

International Journal of Multiphase Flow

www.elsevier.com/locate/ijmulflow

The generalized Kirchhoff equations and their application to the interaction between a rigid body and an arbitrary time-dependent viscous flow

G. Mougin, J. Magnaudet *

Institut de Mécanique des Fluides de Toulouse, UMR CNRS/INPT/UPS 5502, 2, avenue Camille Soula, 31400 Toulouse, France

Received 1 January 2002; received in revised form 18 July 2002

Abstract

Recent numerical and analytical studies have demonstrated that added-mass effects acting on bluff bodies moving in viscous, time-dependent flows are independent of the Reynolds number, acceleration strength and steady/unsteady nature of the flow field. We discuss the origin of this crucial result and show how it can be used to derive the equations governing the motion of a non-deformable body moving freely in an arbitrary time-dependent, viscous flow. Then we show how these equations can be employed in conjunction with the Navier–Stokes equations to solve numerically the coupled problem in which the presence of the body modifies the surrounding flow which itself determines the trajectory of the body. Numerical tests of this coupling are presented. We finally apply the coupled set of equations to analyze the path instability of ellipsoidal bubbles rising at high Reynolds number. We show that numerical results recover the main experimental trends, an agreement suggesting that path instability is primarily driven by the instability of the wake which is itself crucially dependent on the curvature of the bubble surface.
© 2002 Elsevier Science Ltd. All rights reserved.

1. Introduction

During the last decade a considerable effort has been devoted to the numerical investigation of hydrodynamic forces acting on solid particles, liquid drops and gas bubbles. The common aim of such studies is to obtain an accurate description of the forces acting on individual particles in

* Corresponding author.
E-mail addresses: mougin@imft.fr (G. Mougin), magnau@imft.fr (J. Magnaudet).

0301-9322/02/$ - see front matter © 2002 Elsevier Science Ltd. All rights reserved.
PII: S0301-9322(02)00078-2

well-defined flows in order to provide a sound basis for describing complex dispersed flow with a low or moderate volume concentration of the dispersed phase. Most of these numerical studies have considered a *fixed* body submitted to a prescribed flow. This point of view is very efficient for determining the hydrodynamic forces such as quasi-steady viscous drag, added-mass or shear-induced lift. However when this simplification is used, it is not possible to take into account the influence that the force and torque balances over the body surface may have on the global dynamics of the system. For instance, when an ellipsoidal bubble moves into a shear flow, the condition of zero torque imposes a restriction on the orientation of the bubble and this has crucial consequences on its lateral motion (Magnaudet and Eames, 2000). Similarly, it is now clear that the critical Reynolds number beyond which the wake of a solid bluff body becomes unstable and develops vortex shedding is dramatically dependent on the fact that the body is free to move or not (Cossu and Morino, 2000; Govardhan and Williamson, 2000). Hence, to get new insight into the dynamics of freely moving particles or bodies, it is highly desirable to develop a formulation of the problem in which the flow field governed by the Navier–Stokes equations and the motion of the body governed by Newton's laws are considered together. This is the aim of the present contribution. As will be shown later this coupling opens the possibility to describe how wake instabilities affect the trajectory of a rigid body and how in turn the motion of the body may influence wake characteristics.

In the classical framework of inviscid potential flow theory, it is easy to obtain the general equations governing the motion of a non-deformable body of arbitrary shape. This is most easily done by evaluating first the kinetic energy of the whole (body *and* fluid) system and then applying general principles of classical mechanics. The case of a rigid body moving in an unbounded incompressible fluid at rest at infinity was considered more than one century ago by Kirchhoff (see Lamb, 1945, Chapter 6); later, this formulation was extended to the case of bodies moving in steady non-uniform irrotational flows by Taylor (1928). The more general case of a body moving in an arbitrary time-dependent non-uniform irrotational flow was addressed by Landweber and Miloh (1980) and Galper and Miloh (1995) (see also Saffman, 1992, pp. 87–92). In these situations, the motion of the body is completely governed by added-mass effects. The problem becomes much more difficult in presence of viscous effects because vorticity is then generated on the body surface and can be shed in the wake. In this case the forces and torques acting on the body are due to a combination of added-mass effects, skin friction and free vorticity (Howe, 1995). However, DNS studies performed during the last decade (see Magnaudet and Eames, 2000 for a review) have shown that added-mass effects can still be properly defined in a viscous flow (they correspond to the instantaneous change of the hydrodynamic force and torque produced by a relative acceleration between the body and fluid), and that added-mass coefficients are then independent of all flow characteristics such as the instantaneous Reynolds number, Strouhal number, etc. Moreover these studies have also proved that added-mass effects are independent of the nature of the body surface, i.e. they are not affected by changing the no-slip condition at the body surface into a free-slip one or vice versa. This result is extremely important because it allows us to separate conveniently those of the hydrodynamic effects which are due to vorticity (and hence can only be evaluated in general through a numerical solution of the Navier–Stokes equations) from those which result from the kinematic constraint provided by the vanishing of the relative normal velocity at the body surface and are thus described by irrotational flow theory. This is the general framework in which we have analyzed and formulated the general fluid-body problem.

In Section 2 we recall the origin of Kirchhoff's equations for irrotational flows around moving bodies and how these equations can be generalized to viscous, rotational flows. This generalization is made possible by the fact that added-mass contributions are not affected by rotational effects, a crucial result whose origin is discussed in Appendix A. In Section 3 we detail how the Navier–Stokes equations can be written and coupled with the force and torque balances which determine the motion of the body. Section 4 is devoted to a short description of the numerical techniques used to solve the coupled problem and to some tests of this numerical coupling. Finally in Section 5 we apply the material developed before to study the influence that the aspect ratio of an ellipsoidal shear-free bubble rising under gravity may have on the nature of its path. We show that this nature depends crucially on the topology of the near wake of the bubble.

2. Motion of a rigid body through an unbounded fluid

Let us consider a rigid body (B) of mass m, volume $\mathscr{V}$ and centre of mass O moving in an incompressible fluid of density ρ and kinematic viscosity ν, at rest at infinity. We denote by (S_b) (resp. (S_∞)) the body surface (resp. the fictitious outer fluid boundary) and by $\mathbf{U}$ (resp. $\mathbf{\Omega}$) the velocity of the centre of mass (resp. rotation rate) of the body (Fig. 1).

In order that all components of the added-mass tensor be independent of time, we write the governing equations in a frame of reference whose axes rotate at a rate $\mathbf{\Omega}$, so that these axes can always be chosen to be parallel to the principal axes of the body. For the sake of simplicity we restrict our description to bodies with three perpendicular planes of symmetry, but the method applies equally well to general geometries. When such bodies move into an unbounded inviscid fluid at rest at infinity, the kinetic energy of the surrounding fluid may be written in the form (Lamb, 1945, Art. 127):

$$2T = \mathbf{U} \cdot (\mathbb{A}\mathbf{U}) + \mathbf{\Omega} \cdot (\mathbb{D}\mathbf{\Omega}) \tag{2.1}$$

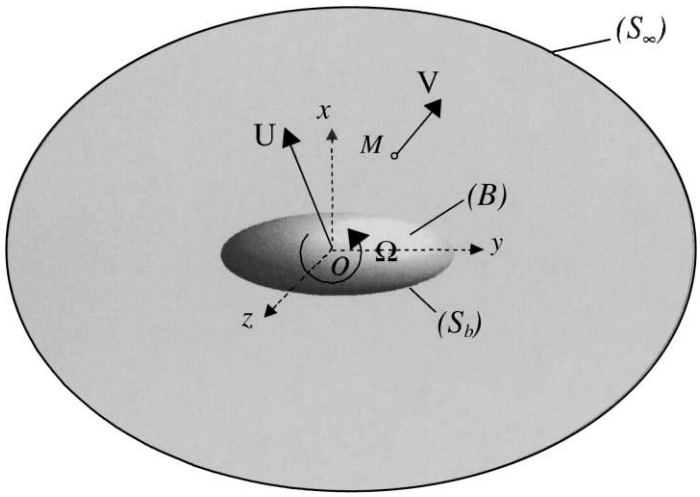

Fig. 1. The fluid-body system.

where $\mathbb{A}$ and $\mathbb{D}$ are second-order diagonal tensors characterizing the mass of fluid set in motion by a translation and a rotation of the body, respectively (with the above notations, $\mathbb{A}$ (resp. $\mathbb{D}$) has the dimension of a mass (resp. a moment of inertia)). Using for instance Lagrange's formalism, one readily obtains Kirchhoff's equations describing the linear and angular momentum balance for the complete fluid/body system (Lamb, 1945, Art. 127) in the form:

$$(m\mathbb{I}+\mathbb{A})\frac{\mathrm{d}\mathbf{U}}{\mathrm{d}t}+\boldsymbol{\Omega}\times((m\mathbb{I}+\mathbb{A})\mathbf{U})=0 \tag{2.2a}$$

$$(\mathbb{J}+\mathbb{D})\frac{\mathrm{d}\boldsymbol{\Omega}}{\mathrm{d}t}+\boldsymbol{\Omega}\times((\mathbb{J}+\mathbb{D})\boldsymbol{\Omega})+\mathbf{U}\times(\mathbb{A}\mathbf{U})=0 \tag{2.2b}$$

where $\mathbb{I}$ is the unit tensor and $\mathbb{J}$ the inertia tensor of the body. In Eqs. (2.2a) and (2.2b) we have assumed that no external force or torque acts on the system but it is well known that such contributions can straightforwardly be added to the right-hand side, provided they result from a conservative process.

In real situations the fluid is viscous and vorticity exists around the body, either because it is generated right at the body surface, or because the body moves in a rotational flow, or both. Existence of vorticity in the flow results in a major difficulty in the analysis of hydrodynamic forces and torques acting on the body because contributions due to the impermeability condition at the body surface act together with those due to the pressure changes induced by vortex forces and those due to viscous effects at the body surface (skin friction). This situation has resulted in many errors and erroneous beliefs, such as empirical "laws" giving the variations of the added-mass coefficients as a function of the flow Reynolds number and Strouhal number (see Magnaudet, 1997 for a short review). This crucial question has only been clarified recently in a combined effort involving DNS studies and analytical contributions aimed to separate properly these various contributions. In a remarkable analysis, Howe (1995) showed rigorously that when a body moves within a viscous, rotational flow at rest at infinity, Kirchhoff's equations can be put within the form:

$$(m\mathbb{I}+\mathbb{A})\frac{\mathrm{d}\mathbf{U}}{\mathrm{d}t}+\boldsymbol{\Omega}\times((m\mathbb{I}+\mathbb{A})\mathbf{U})=\mathbf{F}_\omega+(m-\rho\mathscr{V})\mathbf{g} \tag{2.3a}$$

$$(\mathbb{J}+\mathbb{D})\frac{\mathrm{d}\boldsymbol{\Omega}}{\mathrm{d}t}+\boldsymbol{\Omega}\times((\mathbb{J}+\mathbb{D})\boldsymbol{\Omega})+\mathbf{U}\times(\mathbb{A}\mathbf{U})=\boldsymbol{\Gamma}_\omega \tag{2.3b}$$

where $\mathbf{F}_\omega$ and $\boldsymbol{\Gamma}_\omega$ are the force and torque resulting from the existence of vorticity in the flow, respectively. For the sake of completeness, we have added a buoyancy force due to gravity $\mathbf{g}$ in the right-hand side of Eq. (2.3a) and have assumed that the fluid and the body have constant densities. Howe (1995) also showed how $\mathbf{F}_\omega$ and $\boldsymbol{\Gamma}_\omega$ can be split into two contributions resulting from the effects of free vorticity and skin friction, respectively; this splitting is physically meaningful but it will not be used here because we generally need to obtain $\mathbf{F}_\omega$ and $\boldsymbol{\Gamma}_\omega$ through a numerical solution of the Navier–Stokes equations. The crucial point in Eqs. (2.3a) and (2.3b) is that the added-mass effects can still be properly defined and that the added-mass coefficients (i.e. the components of tensors $\mathbb{A}$ and $\mathbb{D}$) have the same value as in the original Kirchhoff equations (2.2a) and (2.2b). A mathematical justification helping to understand why this is so is given in Appendix A.

3. The governing equations of the fluid-body system

To solve numerically the Navier–Stokes equations around a moving non-deformable body, it is particularly convenient to identify any point M of the space in a system of axes whose origin and directions coincide at any time with the geometric centre O and principal axes of the body, respectively. In this system of axes, M is characterized by a distance vector $\mathbf{r}$ such that $OM = \|\mathbf{r}\|$. The key advantage of this choice is that, when the fluid domain is unbounded externally, the numerical grid does not change with time, so that no remeshing is required. Then, to express the governing equations, the most obvious option would be to introduce the velocity $\mathbf{V}'$ defined relatively to these translating and rotating axes, as is generally done in geophysical fluid dynamics or in flows in turbomachinery. However this choice has some drawbacks in the context of freely moving bodies. For instance, the magnitude of the velocity takes large values far from the body, since $\mathbf{V}'$ must equal $-(\mathbf{U} + \Omega \times \mathbf{r})$ at infinity; this can induce numerical difficulties (in terms of maximum time step) and can lead to poor accuracy. Moreover, the corresponding momentum balance comprises pseudo-forces involving the time-derivatives $\mathrm{d}\mathbf{U}/\mathrm{d}t$ and $(\mathrm{d}\Omega/\mathrm{d}t) \times \mathbf{r}$. Since $\mathbf{U}$ and Ω are two unknowns of the problem that necessarily keep a constant value within each time step (because the geometry of the fluid/body system is temporarily frozen), it is not possible to evaluate accurately these time derivatives directly within the Navier–Stokes equations. To avoid these difficulties, it is more convenient to use another option in which the Navier–Stokes equations are written for the velocity field $\mathbf{V}$ obtained by projecting the *absolute* velocity field $\widetilde{\mathbf{V}}$ onto rotating axes parallel to those defined above but referred to a fixed arbitrary origin $\widetilde{O}$. This choice avoids the problems mentioned above. Moreover it has the advantage that the velocity field coming out from the numerical solution corresponds to the disturbance flow produced by the moving body (because $\mathbf{V}$ tends to zero at large distances) and that the three velocity components can directly be interpreted as the streamwise, cross wise and spanwise components with respect to the instantaneous position of the body.

To obtain the Navier–Stokes equations corresponding to the latter choice we need to combine three results. First, the geometrical velocity at which the control volume centered at M moves is:

$$\mathbf{W} = \mathbf{U} + \Omega \times \mathbf{r}$$

Then, using Leibnitz's rule, the relation between the material derivative of any physical variable ϕ integrated over a control volume $\mathscr{V}_c$ and its derivative following the velocity $\mathbf{W}$ is:

$$\frac{D}{Dt}\int_{\mathscr{V}_c} \phi \mathrm{d}\mathscr{V} = \frac{\partial}{\partial t}\int_{\mathscr{V}_c} \phi \mathrm{d}\mathscr{V}_c + \int_{\partial\mathscr{V}_c} \phi(\mathbf{V} - \mathbf{W}) \cdot \mathbf{n} \mathrm{d}s$$

where $\mathbf{n}$ denotes the outward unit normal to $\partial\mathscr{V}_c$. In local form this yields:

$$\frac{D\phi}{Dt} = \frac{\partial\phi}{\partial t} + (\mathbf{V} - \mathbf{W}) \cdot \nabla\phi = \frac{\partial\phi}{\partial t} + \nabla \cdot (\phi(\mathbf{V} - \mathbf{W}))$$

Third, in the case where $\phi = \widetilde{\mathbf{V}}$ we need to project the latter relation onto the rotating axes. Since the projection of $\partial\widetilde{\mathbf{V}}/\partial t$ on these axes is $\partial\mathbf{V}/\partial t + \Omega \times \mathbf{V}$, we finally obtain the Navier–Stokes equations within the form (Mougin, 2002):

$$\nabla \cdot \mathbf{V} = 0 \tag{3.1a}$$

$$\frac{\partial \mathbf{V}}{\partial t} + \Omega \times \boldsymbol{V} + \nabla \cdot (\mathbf{V}(\mathbf{V} - \mathbf{W})) = \frac{1}{\rho}\nabla P + \nu \nabla^2 \mathbf{V} \tag{3.1b}$$

The associated boundary conditions are (**n** being the local outward unit normal to (S_b)):

$$\mathbf{V} \cdot \mathbf{n} = (\mathbf{U} + \Omega \times \mathbf{r}) \cdot \mathbf{n} \quad \text{on } (S_b) \tag{3.2a}$$

$$\mathbf{n} \times \mathbf{V} = \mathbf{n} \times (\mathbf{U} + \Omega \times \mathbf{n}) \quad \text{on } (S_b) \text{ for a solid body} \tag{3.2b}$$

$$\mathbf{n} \times ((\nabla \mathbf{V} + {}^{\mathrm{T}}\nabla \mathbf{V}) \cdot \mathbf{n}) = 0 \quad \text{on } (S_b) \text{ for a free-slip body} \tag{3.2c}$$

$$\mathbf{V} \to 0 \quad \text{for } \|\mathbf{r}\| \to \infty \tag{3.2d}$$

It is clear that the vorticity-induced force and torque $\mathbf{F}_\omega$ and $\mathbf{\Gamma}_\omega$ of Eqs. (2.3a) and (2.3b) result directly from the integration of the pressure and viscous stress determined by Eqs. (3.1a) to (3.2d). What is less straightforward is to identify the part of the added-mass effects that are included in the pressure field P involved in Eq. (3.1b), keeping in mind that **U** and Ω are kept constant within a time step. To determine these added-mass contributions, let us consider the case where the body (B) is a sphere of radius R translating at a velocity **U** and rotating with a rotation rate Ω such that **U** and Ω, are not parallel. Owing to boundary conditions (3.2a) and (3.2d), the corresponding irrotational solution is:

$$\mathbf{V} = -\frac{1}{2}\left(\frac{R^3}{r^3}\right)\mathbf{U} \cdot \left(\mathbb{I} - 3\frac{\mathbf{rr}}{r^2}\right)$$

because the rotation rate Ω does not induce any fluid displacement for a sphere. Injecting this solution into Eq. (3.1b) and evaluating the pressure field due to the advective contribution $-\nabla.(\mathbf{V}(\Omega \times \mathbf{r}))$ yields after integrating over (S_b):

$$\mathbf{F} = -\rho\left(\frac{\mathscr{V}}{2}\right)\Omega \times \mathbf{U}$$

which is exactly (with a change of sign) the last contribution in the left-hand side of Eq. (2.3a) for the particular case of a sphere ($\mathbb{A} = \rho(\mathscr{V}/2)\mathbb{I}$). Considering bodies for which $\mathbb{D}$ differs from zero and $\mathbb{A}$ is not spherical (for instance ellipsoids), we would similarly conclude that the last two contributions in the left-hand side of the torque balance (2.3b) result from the integration of $-P\mathbf{r} \times \mathbf{n}$ over the body surface. Consequently the only added-mass contributions which are not directly obtained from the integration of (3.1a), (3.1b), (3.2a), (3.2b) over a time interval during which **U** and Ω are kept constant are those corresponding to the time-derivatives $\mathrm{d}\mathbf{U}/\mathrm{d}t$ and $\mathrm{d}\Omega/\mathrm{d}t$. In this sense, integration over (S_b) of the stress $\Sigma_{\mathrm{QS}} = -P\mathbb{I} + \rho\nu(\nabla \mathbf{V} + {}^{\mathrm{T}}\nabla \mathbf{V})$ obtained at time t from (3.1a) to (3.2d) yields the "quasi-static" contribution to the hydrodynamic force and torque, $\mathbf{F}_{\mathrm{QS}}(t)$ and $\mathbf{\Gamma}_{\mathrm{QS}}(t)$ say, defined by:

$$\mathbf{F}_{\mathrm{QS}}(t) = \int_{S_b} \Sigma_{\mathrm{QS}} \cdot \mathbf{n}\mathrm{d}s$$

$$\mathbf{\Gamma}_{\mathrm{QS}}(t) = \int_{S_b} \mathbf{r} \times (\Sigma_{\mathrm{QS}} \cdot \mathbf{n})\mathrm{d}s$$

The terminology "quasi-steady" must however not be misunderstood. It means by no way that $\mathbf{F}_{\mathrm{QS}}$ and $\mathbf{\Gamma}_{\mathrm{QS}}$ do not comprise time-dependent contributions since these force and torque are

obtained by solving the unsteady Navier–Stokes equations for prescribed values of $\mathbf{U}$ and Ω. In particular, unsteady diffusion of vorticity from the surface of the body into the fluid interior contributes to $\mathbf{F}_{QS}$; in the low-Reynolds-number regime this contribution is just the so-called Basset history force. Turning back to Eqs. (2.3a) and (2.3b) we conclude that the correct form of the Kirchhoff equations that must be associated with the flow equations (3.1a) to (3.2d) to determine completely the motion of the body is:

$$(m\mathbb{I} + \mathbb{A})\frac{d\mathbf{U}}{dt} + m\Omega \times \mathbf{U} = \mathbf{F}_{QS}(t) + (m - \rho\mathscr{V})\mathbf{g} \tag{3.3a}$$

$$(\mathbb{J} + \mathbb{D})\frac{d\Omega}{dt} + \Omega \times (\mathbb{J}\Omega) = \mathbf{\Gamma}_{QS}(t) \tag{3.3b}$$

Using the results discussed in Section 2, we know that the components of $\mathbb{A}$ and $\mathbb{D}$ are just those determined by irrotational flow theory, even though we are considering rotational viscous flows, possibly with time-dependent effects.

4. Numerical solution and tests of the coupled problem

The numerical solution of the Navier–Stokes equations (3.1a) and (3.1b) was obtained by adapting the JADIM code already developed in our group; this adaptation consisted in introducing the terms $\Omega \times \mathbf{V}$ and $-\nabla \cdot (\mathbf{VW})$ involved in the left-hand side of Eq. (3.1b). The code solves the three-dimensional unsteady Navier–Stokes equations and has already been thoroughly described in several publications, e.g. Magnaudet et al. (1995), Calmet and Magnaudet (1997) or Legendre and Magnaudet (1998). Let us just mention that the momentum equations are formulated in a general system of orthogonal curvilinear coordinates. The discretization makes use of a staggered mesh and equations are integrated through a second-order time-accurate Runge–Kutta/Crank–Nicolson algorithm. Incompressibility is satisfied at the end of each time step by solving a Poisson equation for an auxiliary potential from which the pressure is deduced. It is important to stress that the velocity field obtained at this stage (say $\mathbf{V}(t + \Delta t)$ where Δt denotes the time step) is the incompressible solution of the full Navier–Stokes equations corresponding to the translational and rotational velocities $\mathbf{V}(t)$ and $\Omega(t)$ that the body had at time t. In other terms, this would be the solution of the complete problem if the values of $\mathbf{V}$ and Ω would not change over time.

Once $\mathbf{F}_{QS}(t + \Delta t)$ and $\mathbf{\Gamma}_{QS}(t + \Delta t)$ are obtained at the end of each time step of length Δt, the modified Kirchhoff equations (3.3a) and (3.3b) are solved using a pseudo-Runge–Kutta scheme. This yields the new values $\mathbf{U}(t + \Delta t)$ and $\Omega(t + \Delta t)$ to be used in the boundary conditions (3.2a)–(3.2c) of the next time step. However, since the time variation $\mathbf{U}(t + \Delta t) - \mathbf{U}(t) = \Delta\mathbf{U}$ and $\Omega(t + \Delta t) - \Omega(t) = \Delta\Omega$ is actually associated with an instantaneous change in the velocity and pressure fields in the whole fluid domain ($\Delta\mathbf{V}$ and ΔP, say), it is necessary to compute this change just after having updated $\mathbf{U}$ and Ω. This is the only way in which the velocity field used at the beginning of the new time step can be made consistent with the kinematic boundary condition (3.2a). To obtain this consistency, we use the results of the analysis detailed in Appendix A and rewrite Eq. (A.6) for $\Delta\mathbf{V}$ in the form:

$$\frac{\Delta \mathbf{V}}{\Delta t} = -\frac{1}{\rho}\nabla(\Delta P) \tag{4.1}$$

From this relation we conclude that ΔP obeys a Laplace equation associated with the boundary condition:

$$\mathbf{n}\cdot\nabla(\Delta P) = -\frac{\rho}{\Delta t}\mathbf{n}\cdot\Delta\mathbf{V} = -\frac{\rho}{\Delta t}(\mathbf{n}\cdot\Delta\mathbf{U} + (\boldsymbol{r}\times\mathbf{n})\cdot\Delta\Omega) \quad \text{on } (S_b) \tag{4.2}$$

Having solved (4.1) and (4.2), we finally compute the velocity and pressure fields $\mathbf{V}+\Delta\mathbf{V}$ and $P+\Delta P$ which are the initial fields of the new time step.

It must be pointed out that, even though all the equations involved in the problem are numerically solved with second-order time-accurate schemes, the time accuracy of the instantaneous values of the resulting force and torque is less. This is due to the fact that the coupling scheme (3.1a), (3.1b), (3.2a)–(3.2d), (3.3a) and (3.3b) combined with Eqs. (4.1) and (4.2) only takes into account the instantaneous, irrotational effects of the changes $\mathrm{d}\mathbf{U}/\mathrm{d}t$ and $\mathrm{d}\Omega/\mathrm{d}t$. Actually these time variations in the boundary conditions also induce a change in the vorticity at the body surface. Physically, during a time step Δt this vorticity diffuses throughout a Stokes layer of thickness $\delta_s(\Delta t) \approx (\nu\Delta t)^{1/2}$ and this diffusion is not taken immediately into account in the present coupling scheme. In the numerical process described above, a vortex sheet is created right at the surface by the velocity change $\Delta\mathbf{V}$ at the end of each time step but the diffusion of this vortex sheet is only taken into account during the next time step. The error induced by this procedure can be rigorously evaluated by examining the short-time behaviour of the Navier–Stokes equations associated with the disturbance $\Delta\mathbf{V}$. This analysis is carried out at the end of Appendix A where we show that the error on the force and torque is $O(\Delta t^{1/2})$ in the case of a solid body and $O(\Delta t)$ for a shear-free body.

To study the flow around axisymmetric bodies, we construct the numerical grid by first generating a plane grid whose outer boundary is a large circle centered at the geometrical centre of the body and then rotating this grid about the axis of symmetry of the body. Most of the computations reported below have been carried out on a grid made of $65\times 59\times 64$ nodes in the meridian, radial, and azimuthal direction, respectively. The grid is highly stretched in the radial direction in order to ensure that at least five grid points lie within the boundary layer surrounding the body. The radius of the fictitious outer boundary is chosen to be 50 times the equivalent radius of the body.

Extensive numerical tests have been carried out in order to make sure that the supplementary terms of Eq. (3.1b) are correctly discretized and that the differential system (3.3a) and (3.3b) is accurately solved. A revealing test consists in giving a rotation Ω about a horizontal axis to a clean (i.e. shear-free) spherical bubble that has already reached its terminal velocity under the effect of gravity. Owing to the spherical geometry of the body, the free-slip boundary condition forces the torque $\mathbf{\Gamma}_{QS}(t)$ on the bubble to be zero at any time. More generally the rotation rate Ω must have strictly not influence on the dynamics of the system and the bubble path must remain vertical and rectilinear. Note that, since Eq. (3.3a) is written in the rotating axes, a constant $\mathbf{U}$ in presence of a non-zero Ω would mean that the bubble would describe open loops. In order to prevent the occurrence of such loops, it is clear that $\mathrm{d}\mathbf{U}/\mathrm{d}t$ must differ from zero and that the force $\mathbf{F}_{QS}(t)$ in the right-hand side of Eq. (3.3a) must contain a term balancing this centripetal acceleration. Obviously the required term is just the added-mass contribution $-\Omega\times(\mathbb{A}\mathbf{U})$. The precision with

Table 1
The rotating spherical bubble after a rotation angle $\|\Omega\|t = 2.45$ ($\|\Omega\| = 1$, $Re = 280$)

Transverse velocity/rise velocity	1.3%
Error on the added-mass coefficient involved in the force $-\Omega \times (\mathbb{A}\mathbf{U})$	0.5%

Table 2
Numerical errors on the added-mass forces and torques on an ellipsoidal bubble

Added-mass contribution	Error
$-\Omega \times (\mathbb{A}\mathbf{U})$	1.2%
$-\Omega \times (\mathbb{D}\Omega)$	0.5%
$-\mathbf{U} \times (\mathbb{A}\mathbf{U})$	1.1%

which this term is taken into account in the coupled resolution of Eqs. (3.1a), (3.1b), (3.2a)–(3.2d), (3.3a) and (3.3b) can be evaluated by measuring the ratio of the transverse (horizontal) velocity to the vertical one. The results presented in Table 1 show that the lateral deviation of the path remains very small, even after the rotation angle has reached large values. Moreover, dividing the horizontal component of $\mathbf{F}_{QS}(t)$ by $\|\mathbf{U}\|\|\Omega\|$ yields the numerical value of the corresponding added-mass coefficient. Table 1 shows that this value is very close to that predicted by irrotational theory. This can be seen as an additional numerical proof that added-mass coefficients are not affected by effects of vorticity and viscosity.

Using a similar technique, all the added-mass contributions contained in Eq. (3.1b), especially those involved in the last two terms of the left-hand side of Eq. (2.3b), have been checked by considering the motion of an oblate bubble with an aspect ratio of 2.05 to which suitable constant velocity $\mathbf{U}$ and rotation rate Ω are applied (gravity is set to zero in these tests). The difference with the analytical value of the corresponding added-mass coefficient is shown in Table 2.

5. An example of application: bubble path instability

Everyday evidence shows that millimetric bubbles rising in low-viscosity liquids do not follow a straight trajectory. Instead, they rise in zigzag (within a given vertical plane) or in helix. Many experiments have been carried out in the past to describe this phenomenon and try to understand its origin (see Magnaudet and Eames, 2000 for a review). However it is only recently that ultrapurification techniques have made possible to study bubbles rising in "pure" water in which the free-slip boundary condition (3.2c) is undoubtedly satisfied. Despite very careful experiments performed with these new techniques (Duineveld, 1995; De Vries, 2001), the mechanism governing the instability of the straight trajectory is not yet clear. This is due in particular to the fact that shape oscillations may obviously exist for large enough bubbles and can interact with other instability mechanisms. They can in particular trigger wake instabilities as was first suggested by Saffman (1956). Even though they are not directly visible, small-amplitude capillary waves can also propagate at the surface of moderate-to-high Reynolds-number bubbles and can similarly promote such interactions. To determine whether or not such shape oscillations or deformations are crucial in the instability mechanism, a good alternative is to perform numerical simulations with idealized bodies mimicking most of the properties of millimetric bubbles except their

small-scale deformability. Since bubbles up to 3–4 mm in diameter rising in water are roughly ellipsoids of revolution (with however a tendency to flatten at the front), the leading-order model for a millimetric bubble is an inertialess oblate spheroid with a prescribed aspect ratio. If such bodies are capable of exhibiting zigzag or helical paths in the same range of Reynolds numbers and aspect ratios as real bubbles, one should probably conclude that small-scale deformations are only a secondary ingredient in the mechanism.

This idealized model can easily be studied with the formulation developed in Section 3 and the numerical code described in Section 4. Here we just present two examples of results obtained through this technique with bubbles of aspect ratio $\chi = 2.05$ and $\chi = 2.5$, respectively. In both cases the Galileo number $Ga = \|\mathbf{g}\|^{1/2} R_{eq}^{3/2}/\nu$ is about 140, where R_{eq} is the equivalent radius of the spheroid (in physical units, this corresponds to a bubble with $R_{eq} = 1.25$ mm rising in water). The bubble is initially at rest and is then set in motion by gravity. A small (typically 10^{-4} **g**) plane periodic disturbance is applied to the gravity field **g**. Fig. 2a clearly shows that no path instability occurs for $\chi = 2.05$.

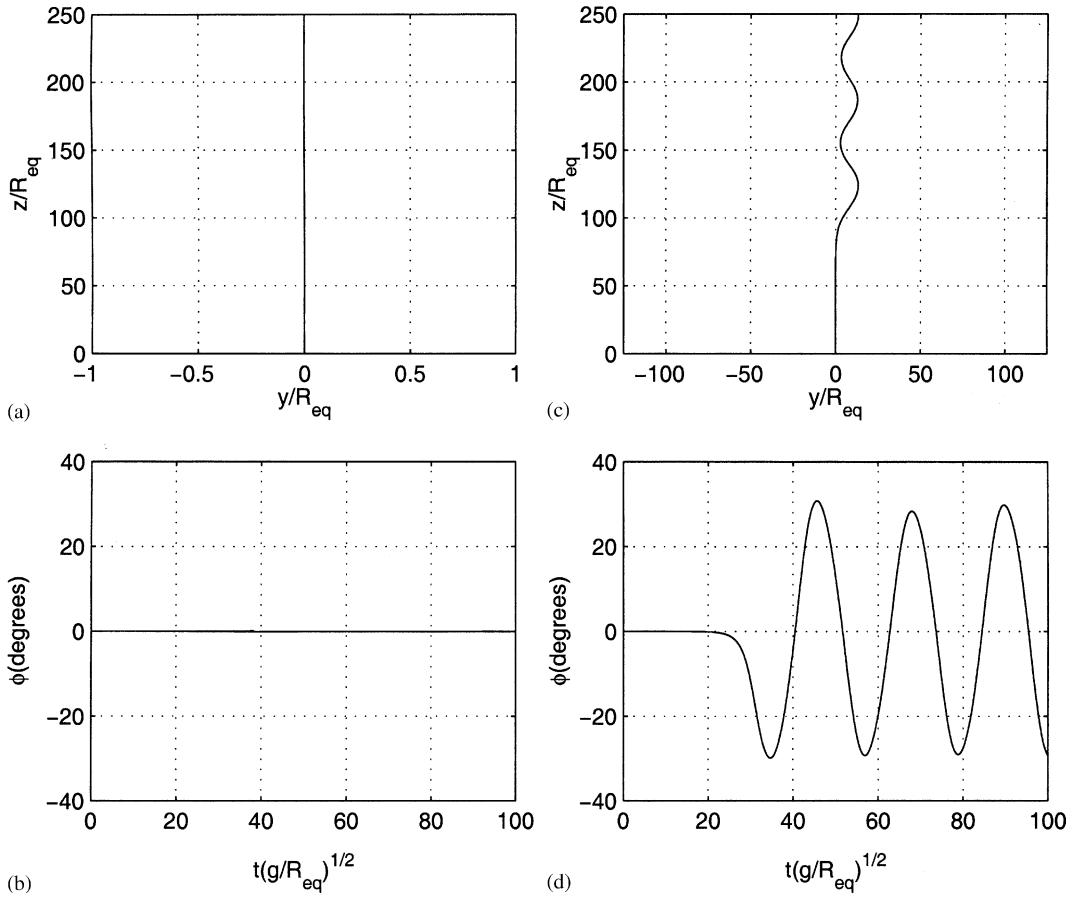

Fig. 2. Path of an ellipsoidal bubble with $Ga = 140$; (a) $\chi = 2.05$; (c) $\chi = 2.5$. Inclination angle of the major axis; (b) $\chi = 2.05$; (d) $\chi = 2.5$.

In the second case ($\chi = 2.5$) the picture is completely different and the bubble now follows a well-defined zigzag path (Fig. 2c) in the plane corresponding to the initial disturbance. The time-averaged rise Reynolds number is about 835 whereas it was about 1515 in Fig. 2a. The angle ϕ between the minor axis of the bubble and the vertical direction oscillates with a frequency $f_N = 4.0$ Hz corresponding to a Strouhal number $St = 2R_{\mathrm{eq}}f_N/U$ about 0.03 (Fig. 2d). Examination of the streamwise vorticity field plotted in Fig. 3 indicates the origin of the difference between the two series of results: while the wake is stable for $\chi = 2.05$ (i.e. almost axisymmetric with only a tiny streamwise component of vorticity due to the body rotation imposed by the perturbation of the gravity field), it is now unstable and vorticity is shed downstream in the form of a well-defined double thread. This wake topology has already been observed in recent experiments (Lunde and Perkins, 1997; De Vries, 2001) in the same range of Reynolds number ($650 < Re < 900$). From the point of view of vorticity dynamics, the main difference between the two cases is that the vorticity generated on the bubble surface is significantly larger for $\chi = 2.5$ than for $\chi = 2.05$ (for large enough aspect ratios, the maximum vorticity on an ellipsoidal bubble increases as $\chi^{8/3}$). Consequently it appears that, for a given Galileo number, there is a threshold χ_c beyond which the flow is not able anymore to evacuate vorticity just by an axisymmetric transport/stretching process. In addition to the wake structure, other characteristics of this second case such as the frequency of the zigzag motion and the rise Reynolds number are typically in the range of experimental observations. Quantitative differences with observations may however exist in χ_c as well as in the frequency for many reasons. For instance surfactants are probably present in most experiments (such as those of Lunde and Perkins, 1997 and Ellingsen and Risso, 2001) and they probably lower somewhat χ_c. Capillary oscillations may result in the same tendency by increasing locally

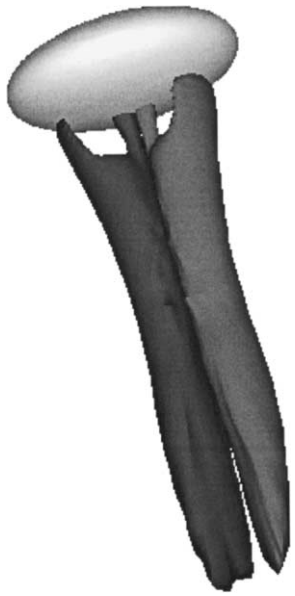

Fig. 3. Isosurface $\omega_x R_{\mathrm{eq}}/U_\infty = \pm 0.7$ of the streamwise vorticity in the wake of an ellipsoidal bubble ($\chi = 2.5$, $Re = 835$).

the curvature of the surface and hence increasing the maximum vorticity. Nevertheless it appears that vorticity generation on a curved shear-free surface coupled with the anisotropic added-mass effects associated with ellipsoids is able to reproduce qualitatively the main trends displayed by recent experiments. The results discussed in this section are only part of the more general analysis of the path instability of a rising bubble that we are currently exploring. In particular, the present model also reproduces the transition from the zigzag path to the helical path which is also frequently observed in experiments. More details about the application of the present model to this fascinating physical problem may be found in the recent paper by Mougin and Magnaudet (2002).

6. Conclusion

In this work we have derived a rigorous method for coupling the Navier–Stokes equations describing the flow field around a rigid, freely moving body with the force and torque balances governing the motion of the body itself. This method is based on the central and now well-established result that added-mass coefficients are independent on the strength of rotational effects, including those due to viscosity. Systematic tests of the numerical implementation of this technique have been reported. They show that added-mass effects are accurately captured by the numerical scheme. An evaluation of the time accuracy of the global coupling has also been carried out. Finally we have shown how the whole technique applies to the study of path instability of a high-Reynolds-number rising bubble. It turns out that the amount of vorticity generated by the shear-free condition on the curved surface of the bubble is a crucial ingredient of the problem. Below some critical aspect ratio of the bubble, this amount is moderate and the bubble rises along a straight vertical path. In contrast, beyond a given threshold, vorticity is shed in the wake in the form of a double thread. In the latter regime the bubble follows a zigzag or helical motion characterized by a low-frequency oscillation. These results are in good qualitative agreement with those of recent experiments and show that the present coupling technique opens new possibilities for studying the subtle coupling mechanisms existing between wake instabilities and trajectories of freely moving bodies.

Appendix A

To understand physically why the added-mass contribution is not affected by rotational effects, let us consider the following example. The body (B) is assumed to be fixed and is surrounded by a time-dependent rotational flow whose velocity and pressure fields are $\mathbf{V}(\mathbf{x},t)$ and $P(\mathbf{x},t)$, respectively. Far upstream from the body the flow is assumed to have a uniform time-dependent velocity; at time $t=t_0$ this upstream velocity is $\mathbf{V}_\infty$. During the time interval $[t_0,t_0+\Delta t]$, the upstream velocity experiences a change characterized by a constant acceleration α in a direction whose unit vector is $\mathbf{e}_\alpha$. Thus, setting $\mathbf{V}(\mathbf{x},t_0+\tau)=\mathbf{V}(\mathbf{x},t_0)+\mathbf{v}'(\mathbf{x},\tau)$ and $P(\mathbf{x},t_o+\tau)=P(\mathbf{x},t_0)+p'(\mathbf{x},\tau)$ for $\tau\in[0,\Delta t]$, the disturbance field $(\mathbf{v}',p')$ satisfies the set of equations:

$$\nabla\cdot\mathbf{v}'=0 \tag{A.1}$$

$$\frac{\partial \mathbf{v}'}{\partial t} + \mathbf{V}\cdot\nabla\mathbf{v}' + \mathbf{v}'\cdot\nabla\mathbf{V} + \mathbf{v}'\cdot\nabla\mathbf{v}' = -\frac{1}{\rho}\nabla p' + \nu\nabla^2\mathbf{v}' \tag{A.2}$$

$$\mathbf{v}' \to \alpha(t-t_0)e_\alpha \quad \text{for } \mathbf{r}\cdot\mathbf{e}_\alpha \to -\infty \tag{A.3}$$

$$\mathbf{v}'\cdot\mathbf{n} = 0 \quad \text{on } (S_\mathrm{b}) \tag{A.4}$$

$$\mathbf{n}\times\mathbf{v}' = 0 \quad \text{on } (S_\mathrm{b}) \tag{A.5}$$

where we have assumed that the flow obeys a no-slip condition at the body surface. To determine the order of magnitude of the various terms involved in the momentum equation (A.2), we introduce three dimensionless parameters, namely $Ac = \alpha R/V_\infty^2$, $Re = RV_\infty/\nu$, and $\varepsilon = \alpha\Delta t/V_\infty$, where $V_\infty = \|\mathbf{V}_\infty\|$ and R is a typical lengthscale of the body. Normalizing each term of Eq. (A.2) by V_∞^2/R, we can conclude that the time-rate-of-change of $\mathbf{v}'$ is $\mathrm{O}(Ac)$ whereas the first two advective terms are $\mathrm{O}(\varepsilon)$ and the third advective term is $\mathrm{O}(\varepsilon^2)$. The viscous term requires some more attention because, owing to the boundary condition (A.5), the variation of the upstream conditions between $t = t_0$ and $t = t_0 + \Delta t$ induces a Stokes layer of thickness $\delta_\mathrm{s}(\Delta t) \approx (\nu\Delta t)^{1/2}$ around the body. Within this Stokes layer whose thickness can be rewritten within the dimensionless form $\delta_\mathrm{s}(\Delta t)/R \approx (\varepsilon/ReAc)^{1/2}$, the viscous term is $\mathrm{O}(Ac)$. In contrast, outside the Stokes layer, this term is only $\mathrm{O}(\varepsilon/Re)$. The analysis of the disturbance flow within the Stokes layer is modified if instead of the no-slip condition (A.5) we consider a shear-free boundary condition. In this case the vorticity disturbance at the body surface is twice the product of the local curvature H of the surface in the flow direction by the tangential velocity disturbance (Batchelor, 1967, p. 366). Hence introducing the dimensionless curvature $\eta = RH$ we see that the dimensionless surface vorticity is $\mathrm{O}(\varepsilon\eta)$. From this it follows that within the Stokes layer (whose thickness is unchanged), the viscous term of Eq. (A.2) is now $\mathrm{O}(\eta(\varepsilon Ac/Re)^{1/2})$, i.e. it is smaller than in the case of a no-slip surface by $\mathrm{O}(\eta(\varepsilon/AcRe)^{1/2})$.

Now let us consider the limit $\Delta t \to 0$, i.e. $\varepsilon \to 0$. From the foregoing analysis we conclude that everywhere (except right on the surface of the body in the case of a no-slip condition), the disturbance flow $(\mathbf{v}', p')$ is governed by the momentum equation:

$$\frac{\partial \mathbf{v}'}{\partial t} = -\frac{1}{\rho}\nabla p' \tag{A.6}$$

Eqs. (A.1) and (A.6) supplemented by boundary conditions (A.3) and (A.4) are just those defining a potential flow around (B). Hence we conclude that, whatever Re and Ac, the short-time behaviour of the disturbance produced by a change in the upstream flow conditions is that predicted by potential flow theory. Consequently, the short-time changes experienced by the force and torque acting on the body correspond to the irrotational added-mass effects produced by the upstream condition (A.3). The above reasoning holds whatever the geometry of the body and it can obviously be generalized to any kind of change in the upstream velocity, i.e. to any translation or rotation. The same reasoning also holds if, instead of a change in the upstream conditions, we consider a change in the kinematic condition (A.4), i.e. a variation in $\mathbf{U}$, Ω, or in the orientation of the body. The hydrodynamical interpretation of this general result is that the short-time disturbance produced by a non-deformable body moving in an incompressible unbounded flow is always dominated by the effect of the dipole associated with the body, irrespective of the strength of rotational and viscous effects (Magnaudet and Eames, 2000).

Having found the leading-order contribution to the force and torque, we can also use the above order-of-magnitude analysis to evaluate the strength of the next contribution. First, using Green's theorem, the contribution of the advective terms in (A.2) can be expressed in the form of surface integrals on (S_b) and (S_∞). The kinematic condition (A.4), the solenoidality of $\mathbf{v}'$ and $\mathbf{V}$, and the vanishing of velocity gradients $\nabla\mathbf{v}'$ at infinity lead to the conclusion that only the term $\int_{S_\infty} \mathbf{V}\mathbf{v}' \cdot \mathbf{n}\mathrm{d}S$ contributes to the resulting force and torque. Using the same normalization as above, the added-mass force and torque are $O(Ac)$ and the advective contribution just mentioned is $O(\varepsilon)$. Similarly, the contribution of viscous effects coming from the bulk of the flow is $O(\varepsilon/Re)$. Finally the contribution of viscous effects near the body can be obtained by integrating the corresponding viscous term over the non-dimensional volume of the Stokes layer, that is $O((\varepsilon/ReAc)^{1/2})$. Hence we find that the contribution of the Stokes layer to the force and torque is $O((\varepsilon Ac/Re)^{1/2})$ in the case of a no-slip boundary condition whereas it is only $O(\eta(\varepsilon/Re))$ in the case of a shear-free surface. From this analysis we conclude that in the limit $\varepsilon \to 0$, the leading-order error made in the evaluation of forces and torques by replacing the complete equation (A.2) by (A.6) is $O((\varepsilon/ReAc)^{1/2})$ for a solid body and $O(\mathrm{Max}(\varepsilon, \varepsilon/Re, \eta\varepsilon/Re))$ for a shear-free body. Hence in the case of a solid surface this leading-order error always come from the fact that diffusion of vorticity within the Stokes layer is neglected during the time interval Δt in (A.6). In contrast, the leading-order error generally comes from the advective term, i.e. from advection and stretching of vorticity in the far wake, for high-Reynolds-number shear-free bubbles; nevertheless the error is smaller than in the no-slip case.

References

Batchelor, G.K., 1967. An Introduction to Fluid Dynamics. Cambridge University Press, Cambridge.

Calmet, I., Magnaudet, J., 1997. Large-eddy simulation of high-Schmidt number mass transfer in a turbulent channel flow. Phys. Fluids 9, 438–455.

Cossu, C., Morino, L., 2000. On the instability of a spring-mounted circular cylinder in a viscous flow at low Reynolds numbers. J. Fluids Struct. 14, 183–196.

De Vries, A., 2001. Path and wake of a rising bubble. Ph.D. thesis. Twente Univ., The Netherlands.

Duineveld, P.C., 1995. The rise velocity and shape of bubbles in pure water at high Reynolds number. J. Fluid Mech. 292, 325–332.

Ellingsen, K., Risso, F., 2001. On the rise of an ellipsoidal bubble in water: oscillatory paths and liquid induced velocity. J. Fluid Mech. 440, 235–268.

Galper, A., Miloh, T., 1995. Dynamic equations of motion for a rigid or deformable body in an arbitrary non-uniform potential flow field. J. Fluid Mech. 295, 91–120.

Govardhan, R., Williamson, C.H.K., 2000. Modes of vortex formation and frequency response of a freely vibrating cylinder. J. Fluid Mech. 420, 85–130.

Howe, M.S., 1995. On the force and moment on a body in an incompressible fluid, with application to rigid bodies and bubbles at low and high Reynolds numbers. Q.J. Mech. Appl. Math. 48, 401–426.

Lamb, Sir H., 1945. Hydrodynamics, sixth ed. I, Dover, New York.

Landweber, L., Miloh, T., 1980. Unsteady Lagally theorem for multipoles and deformable bodies. J. Fluid Mech. 96, 33–46.

Legendre, D., Magnaudet, J., 1998. The lift force on a spherical bubble in a viscous linear shear flow. J. Fluid Mech. 368, 81–126.

Lunde, K., Perkins, R., 1997. Observations on wakes behind spheroidal bubbles and particles. Proc. ASME Fluids Eng. Div. Summer Meeting, paper 97–3530, Vancouver, Canada.

Magnaudet, J., 1997. The forces acting on bubbles and rigid particles. Proc. ASME Fluids Eng. Div. Summer Meeting, paper 97–3522, Vancouver, Canada.

Magnaudet, J., Eames, I., 2000. The motion of high-Reynolds-number bubbles in inhomogeneous flows. Ann. Rev. Fluid Mech. 32, 659–708.

Magnaudet, J., Rivero, M., Fabre, J., 1995. Accelerated flow past a rigid sphere or a spherical bubble. Part I. Pure straining flow. J. Fluid Mech. 284, 97–135.

Mougin, G., 2002. Interaction entre la dynamique d'une bulle et les instabilités de son sillage. Ph.D. Dissertation, Institut National Polytechnique, Toulouse.

Mougin, G., Magnaudet, J., 2002. Path instability of a rising bubble. Phys. Rev. Lett. 88, paper number 014502.

Saffman, P.G., 1956. On the rise of small air bubbles in water. J. Fluid Mech. 1, 249–275.

Saffman, P.G., 1992. Vortex Dynamics. Cambridge University Press, Cambridge.

Taylor, G.I., 1928. The forces on a body placed in a curved or converging stream of fluid. Proc. Roy. Soc. London A 120, 260–283.